Chapter 3

Solution-Processed Ag-TiO_2 Nanostructure-Based Schottky Junction Thin Films for Narrowband Hot-Electron Photodetectors

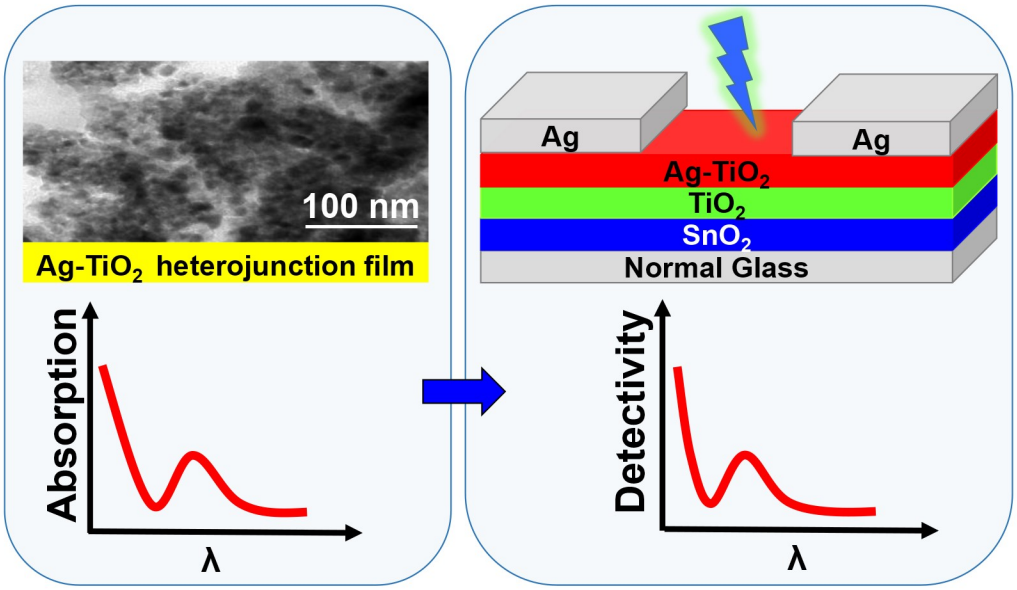

Chapter 3

This chapter mainly focuses on the results of plasmonic NPs based hot electron photodetector. It is not very easy to capture plasmonic hot electrons for photodetection in a photodetector. In this work, an in-situ grown Ag-TiO_2 nano-schottky junction thin film has been deposited by solution processed technique which contains a highly dense Ag NPs surrounded by TiO_2. This Ag-TiO_2 nano-Schottky junction has a low barrier height, high interface area with least interface state that enables efficient hot electron transfer to the CB of TiO_2, which is realized in the EQE data. This EQE data shows an intense photocurrent formation in the region of plasmonic absorption of Ag NP, indicating the primary contribution of hot electrons on photocurrent production. This photodetector has been fabricated in a glass substrate in photoconductor geometry that shows a peak detectivity of 3.19×10^{11} Jones at 420 nm with a response time of ~ 2 sec.

3.1 Introduction

Plasmonic hot-electrons are energetic electrons which are produced by the decay of surface plasmons in metal nanostructured materials.[144] A suitable combination of metal NP and semiconductor can form a low barrier height Schottky junction that can efficiently transfer plasmon induced hot electrons to the semiconductor, which convert photons to other forms of energy.[145, 146] A number of reports claim that the barrier height of these nano-Schottky junctions is much lower w.r.t their bulk combination, which also can be tuned by changing their nanostructure. These plasmatic hot electrons possess a broad range of applications, including photo-catalysis, photo-electrochemical water splitting, photovoltaic conversion, photodetection and so on.[147-150] The plasmonic hot electron-induced photocurrent needs to transfer to the semiconducting layer efficiently for its photovoltaic and photodetection application.[81, 151] Besides, the plasmonic absorption spectra depends on the shape and size of metal NPs and commonly shows a narrow band absorption for similar size metal

NPs.[152, 153] Therefore, a narrowband photodetector can be fabricated by efficient detection of a plasmonic hot electron and detection spectra can be tuned by varying the nanostructure.[154-156] However, due to the inefficient hot-electron charge transfer rate to the semiconducting layer, until now most of the plasmonic photodetectors show too poor detectivity to detect. In fact, most of the claim of plasmonic hot electron photodetector doesn't show EQE data to show the intense photocurrent generation in the plasmonic absorption region of the materials. Although, without showing this data, it's difficult to estimate the real contribution of hot electron in the overall photocurrent.

To date, most plasmonic hot electron photodetectors are based on Au/semiconductor Schottky diodes mainly because of the very high stability of Au nanoparticles.[157-159] Although, Ag NPs are very cost-effective metal and assumed to be a superior plasmonic element than Au because of their efficient surface plasmon effect. Besides, their plasmonic resonance wavelengths exist in the range of 400–480 nm and can have quite good stability. Hot electrons are formed in Ag nanocrystals through intraband excitation inside the conduction band (from occupied s-band to vacant s-band) due to its stronger intraband transition.[68, 72, 160] On the other hand, among different metal oxide semiconductors, n-type TiO_2 is considered as an attractive choice for various applications like electrochemical, photochemical and photovoltaic due to its extremely high physical and chemical durability.[161, 162] Besides, it is also commonly used as electron-accepting semiconductor in different heterostructure device where photo-generated electrons are required to separate promptly.[163, 164] Particular in Ag/TiO_2 heterostructure, energy band off-set for electron is quite low, which enable to transfer electron from Ag to the CB of TiO_2 very efficiently.[165] Therefore, Ag-TiO_2 heterostructure has been widely used for various applications including, photo-catalyst, photo-electro-catalysis, photodetectors, solar cell etc.[140, 166, 167] However, till now, there are very few reports where metal NPs are incorporated into TiO_2 nanostructures for the use of a plasmonic hot electron-based photodetector.[168] In most of the photodetector fabrication, expensive transparent electrode like indium tin oxide (ITO) or fluorine doped tin oxide (FTO) are used as substrate.[169] Besides, different physical vapor deposition techniques are used for such plasmonic photodetector fabrication which increases overall cast of fabrication.[170]

In this chapter, We fabricated an in-situ grown Ag-TiO_2 plasmonic hot electron photodetector fabrication through a solution processed technique where highly dense Ag NPs are embedded by TiO_2 semiconductor. To improve photodetector device performance, a TiO_2/SnO_2 heterojunction thin film is used as an underlying layer of this Ag-TiO_2 nanocrystals thin film. This photodetector has a fast response speed with a good narrowband detectivity that originated from plasmonic hot electron induced photocurrent and it is shown that the LSPR emission by Ag NPs and their subsequent transfer to the TiO_2 matrix by analyzing narrowband EQE of the device. To differentiate the removal of hot electrons by intraband excitation, EQE, absorption/reflection spectra and internal quantum efficiency (IQE) are investigated. An empirical model based on the energy band diagram has been proposed to explain the working principle and the underlying photo-physics of the device.

3.2 Experimental Section

3.2.1 Synthesis of Materials

The ion-conducting LTO dielectric, SnO_2, and TiO_2 semiconductors have been synthesized by a low-cost solution process technique. The detailed synthesis method is described in **Chapter 2 Sections 2.1.1, 2.1.2** and **2.1.5**, respectively.

3.2.2 Growth of Ag-TiO_2 Thin Film and Device Fabrication

The photodetector has been fabricated on a glass substrate in a photoconductor geometry and the fabrication steps of this device has been explained **Chapter 2 Section 2.3.1**, and schematically present in **Figure 2.6**. Four different type of device structure has been developed, which is shown in **Figure 3.1a-d)**. In each device, Ag electrodes (effective area ~ 0.84×0.84 mm^2) are deposited on top by thermal evaporation through a shadow mask technique.

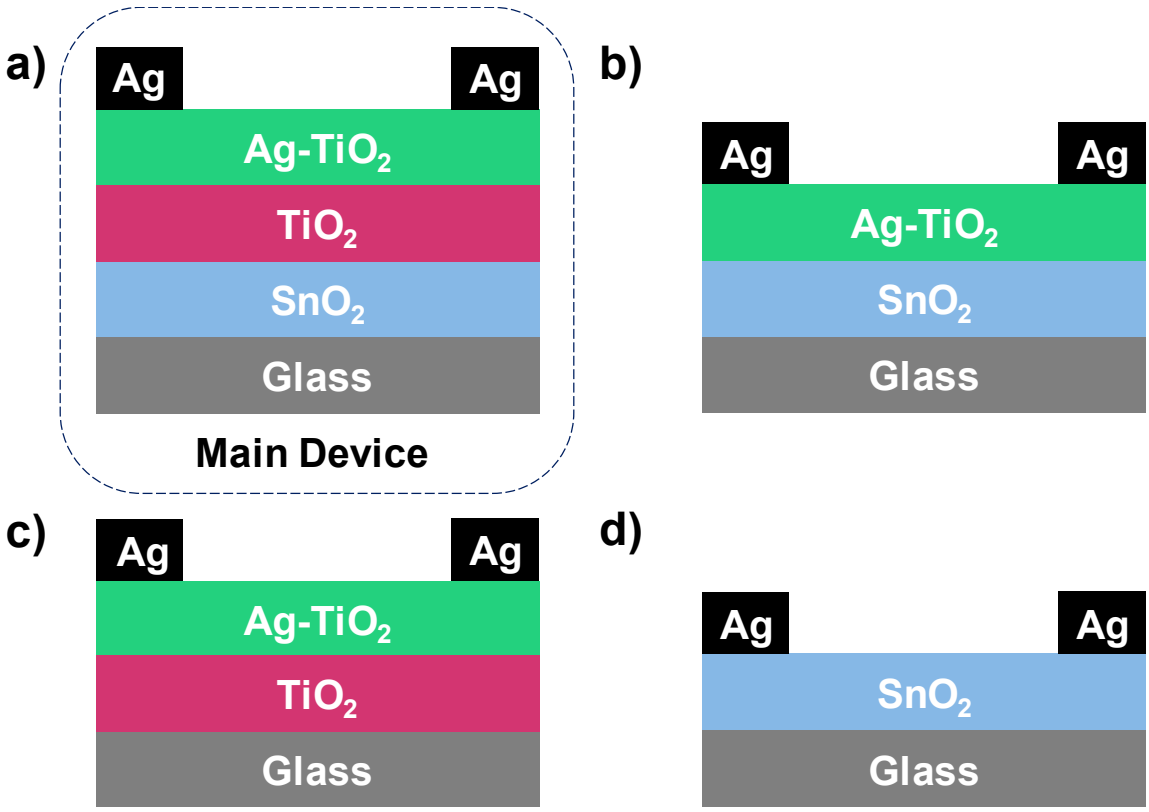

Figure 3.1 Schematic presentation of four different device structure **a)** Ag-TiO_2/TiO_2/SnO_2 layer (proposed device) **b)** with Ag-TiO_2/SnO_2 layer **c)** with Ag-TiO_2/TiO_2 layer **d)** with SnO_2 layer only**.**

3.3 Result and discussion

3.3.1 XRD, UV-Vis and PL Study

Step-by-step XRD pattern of Ag-TiO_2/TiO_2/SnO_2 thin films are depicted in **Figure 3.2a)**. The glass substrate is used as a reference, and the XRD data of the bare glass is subtracted from sample data to get the actual signal of the sample. The XRD pattern of the SnO_2 thin film annealed at 500˚C exhibits peaks generated from the (110), (101), (200), (211), and (310) planes which are located at 2θ of 26.31˚, 33.58˚, 37.55˚, 51.39˚ and 54.32˚ respectively (JCPDS file no. 411445). The thin-film XRD pattern of SnO_2/TiO_2 gives two additional intense peaks at 2θ ~25.01˚ and 47.76˚ which corresponds to (101) and (200) of TiO_2 (JCPDS file no. 2111272), indicating the anatase phase formation of TiO_2. Similarly, LTO/ SnO_2/TiO_2 film shows an additional intense peak at 2θ ~ 44.79˚ corresponds to LTO (400)

well matched with JCPDS file no. 490207. In case of multilayer device structure, we get all XRD peaks including the intense (111) & (200) planes of Ag NPs located at 2θ ~ 37.96˚ and 43.58˚ respectively (JCPDS file no. 897322). For optical studies, thin films of pure LTO, Ag-TiO_2, and Ag-TiO_2/TiO_2/SnO_2 are fabricated on a quartz substrate using the same conditions as used in photodetector fabrication. The normalized UV-Vis absorbance spectra of pure $Li_4Ti_5O_{12}$, Ag-TiO_2, and Ag-TiO_2/TiO_2/SnO_2 thin films spanning the optical spectral region of 300–800 nm are shown in **Figure 3.2b)**. The absorption spectrum of Ag-TiO_2 thin film demonstrates narrowband plasmonic absorption of Ag NPs with a plasmonic peak at 420 nm in visible range of spectra. This plasmonic absorption produces hot electrons which can be utilized for fabrication narrowband photodetectors. Furthermore, we investigated the optical transparency and reflectivity of Ag-TiO_2/TiO_2/SnO_2/glass stacked film which is shown in **Figure 3.2c)**, indicating an excellent optical transparency of 80-85% in the visible region. In addition, it also indicates that the reflectivity of the film is relatively higher (~35%) in the range of 300-400 nm compared to longer wavelength (~20%). The PL spectra of the Ag-TiO_2 thin film is shown in **Figure 3.2d)**, which is acquired in the range of 350-600 nm with an excitation wavelength of 350 nm, indicating the emission peaks around 405 nm (3.06 eV), which is related to a band-to-band transition of TiO_2 semiconductor in the UV region.

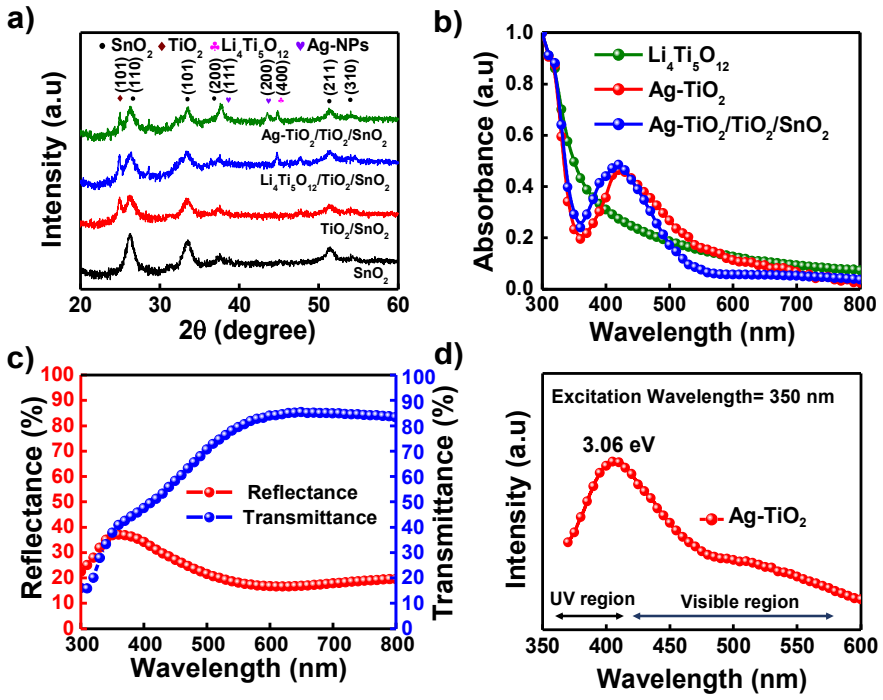

Figure 3.2a) Step-by-step XRD pattern of proposed thin film (Ag-TiO_2/TiO_2/SnO_2) **b)** UV-Vis absorption spectra of LTO,Ag-TiO_2 and Ag-TiO_2/TiO_2/SnO_2 thin films **c)** optical transparency and reflectance of Ag-TiO_2/TiO_2/SnO_2 **d)** PL emiossion spectra of Ag-TiO_2 with the excitation wavelength of 350 nm.

3.3.2 Surface Morphology (HR-SEM & HR-TEM) Study

The surface morphology of Ag-TiO_2 is studied in detail using HR-SEM, as illustrated in **Figure 3.3a)**. From this picture, it can be noted that the formation of densely packed bright spots, which originated from Ag NPs, is surrounded by relatively low intensity zones, indicating the growth of Ag NPs inside a TiO_2 matrix. This difference of contrast appears in the SEM image because of the difference in electron density. As Ag NPs have higher electron density, it becomes much brighter than TiO_2, and makes it easily distinguishable. This data also revealed that the particle sizes of Ag NPs are within the ranges between 5 to 35 nm with an average particle size of ~16 nm **Figure 3.3b)**. An energy-dispersive X-ray spectrometer (EDX) connected to the HR-SEM determines the chemical compositions of the metallic elements that clearly demonstrates the presence of Ag and Ti components within the thin film **Figure 3.3c)**. The color mapping of Ag-TiO_2 thin film is shown in the **Figure 3.3d)**, indicating the uniform distribution of Ag, Ti and O ions.

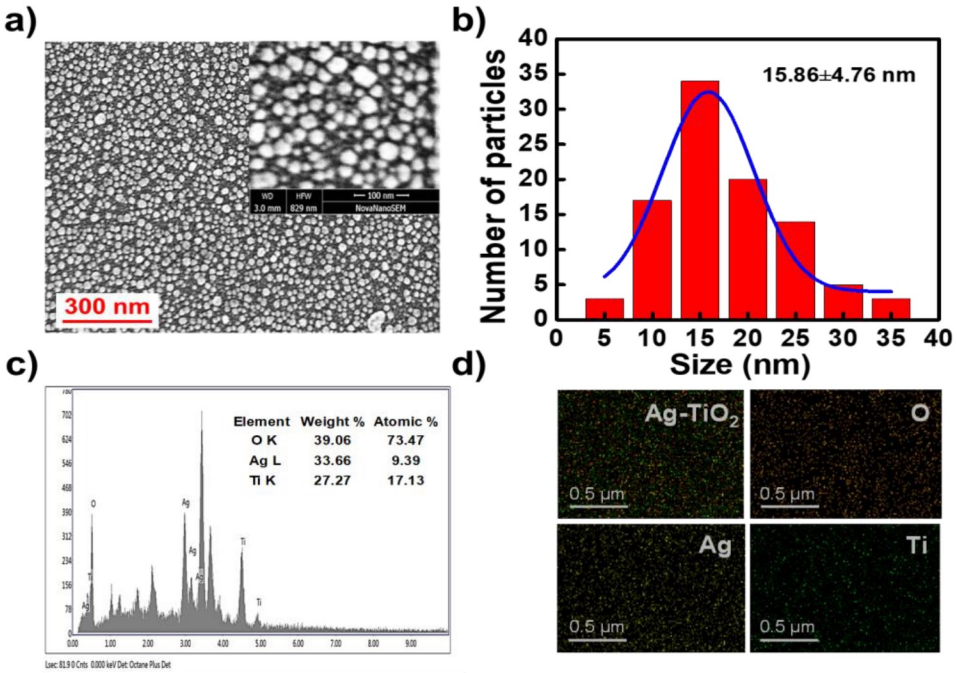

Figure 3.3a) HR-SEM image of Ag-TiO_2 thin film **b)** particle size distribution of Ag (NPs) inside TiO_2 thin film **c)** EDX elemental analysis **d**) color mapping image of Ag-TiO_2 thin film.

TEM analysis of the Ag (NPs)-TiO_2 nanocomposites has been performed for further structural analysis, as illustrated in **Figure 3.4**. For the TEM sample preparation, Ag-TiO_2 thin film is scratched out with the help of a clean glass slide and collected on a clean paper. Then, it is dissolved in isopropanol and dispersed with the help of a probed sonicator for a few minutes. Subsequently a 10 μL drop of this dispersed solution is collected into a TEM grid and used for further analysis. **Figure 3.4a)** shows that the Ag-NPs have been grown quite uniformly within the TiO_2 matrix. This data also shows that NPs are predominantly between 5 and 25 nm in size, with an average particle size of 15.2 nm, which is consistent with the HR-SEM study. The particle size distribution of Ag NPs inside TiO_2 matrix is shown in **Figure 3.4b)**. Higher magnification TEM analysis **Figure 3.4c)** of an Ag-TiO_2 sample indicates individual lattice fringe formation of Ag-NPs and TiO_2, implying their own co-existence. The average d-spacing of Ag-NPs and TiO_2 are 0.203, 0.241, and 0.352 nm, respectively which are corresponding to the Ag (200), Ag (111) and anatase TiO_2 (101) planes. All this spacing's are also defined by the selected area electron diffraction pattern (SAED), as shown in **Figure 3.4d)**. As shown earlier, the XRD pattern of the Ag-TiO_2 sample (**Figure 3.2a)**) also revealed the same set of planes.

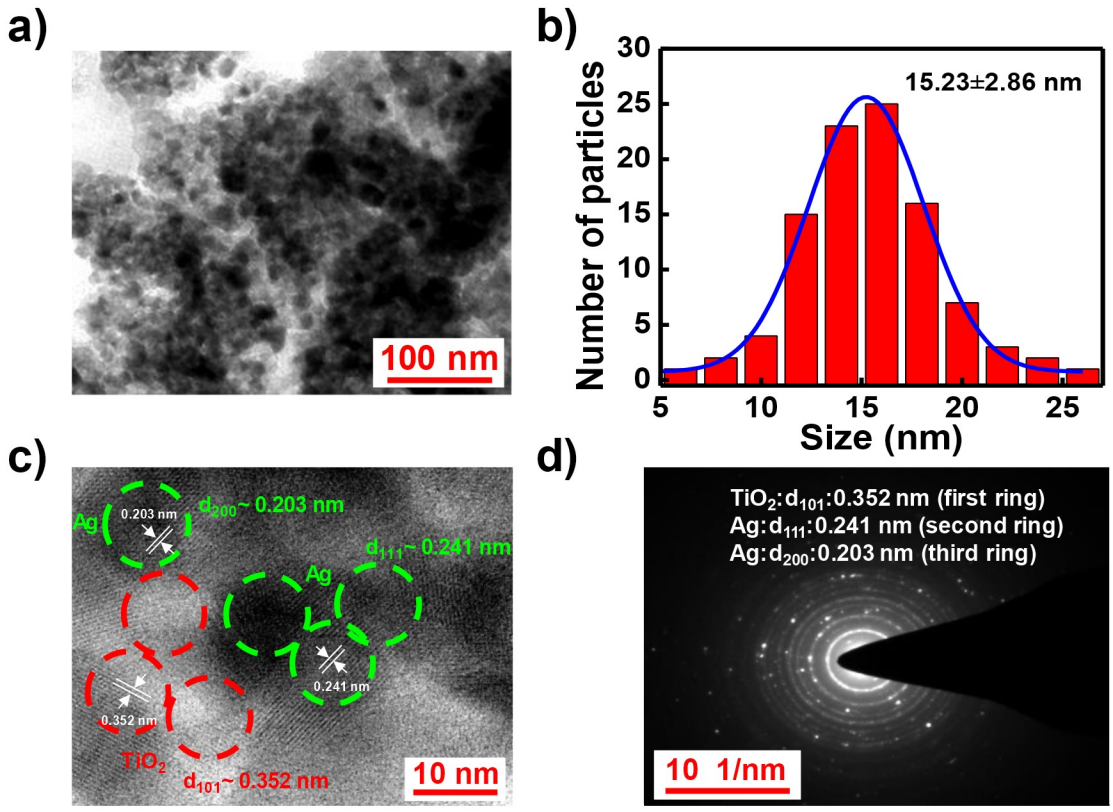

Figure 3.4a) TEM image of Ag-TiO_2 thin film **b)** distribution of particle size of Ag-NPs from TEM image analysis **c)** high-resolution image of Ag (NPs)-TiO_2, greenish ring suggests the lattice d-fringe of Ag NPs and reddish ring for TiO_2 **d)** SAED pattern of Ag (NPs)-TiO_2.

3.3.3 Photodetection Under Dark and Light

Top Ag electrodes of size 0.84 × 0.84 mm^2 which are separated by 200 µm, works as contacts for all electrical characteristics. The electrical current-voltage (I-V) characteristics of multi-layer heterojunction and single-layer photoconductors are measured at room temperature under dark and white lamp illumination conditions, as shown in **Figure 3.5a-d)** respectively. A high-power Xenon lamp that works as source of white light has been illuminated from the top of the device (inset of **Figure 3.5a-d)**). For heterojunction proposed device, light intensity has been varied from 20 W/m^2 to 800 W/m^2 and it is observed that under ±10 V external bias dark current density is ~10^{-3} A/cm^2 which increased by 416 times under the illumination of 800 W/cm^2 light. In comparison to that, under same light illumination (800 W/m^2), enhancement of current for Ag-TiO_2/SnO_2 and Ag-TiO_2/TiO_2 based device shows a

less photocurrent generation, indicating the crucial role of TiO_2/SnO_2 heterojunction as a bottom layer of the device. On the other hand, only SnO_2 semiconductor-based device shows ~two orders less photocurrent generation. For optimization, we varied the initial concentration of Ag-TiO_2 layer and 300 mM concentrated Ag-TiO_2 layer shows better photocurrent generation compared to others. I-V characteristics with different concentration of Ag-TiO_2 (100 mM, 200 mM, 500 mM) thin film is shown in **Figure 3.6a-c)**.

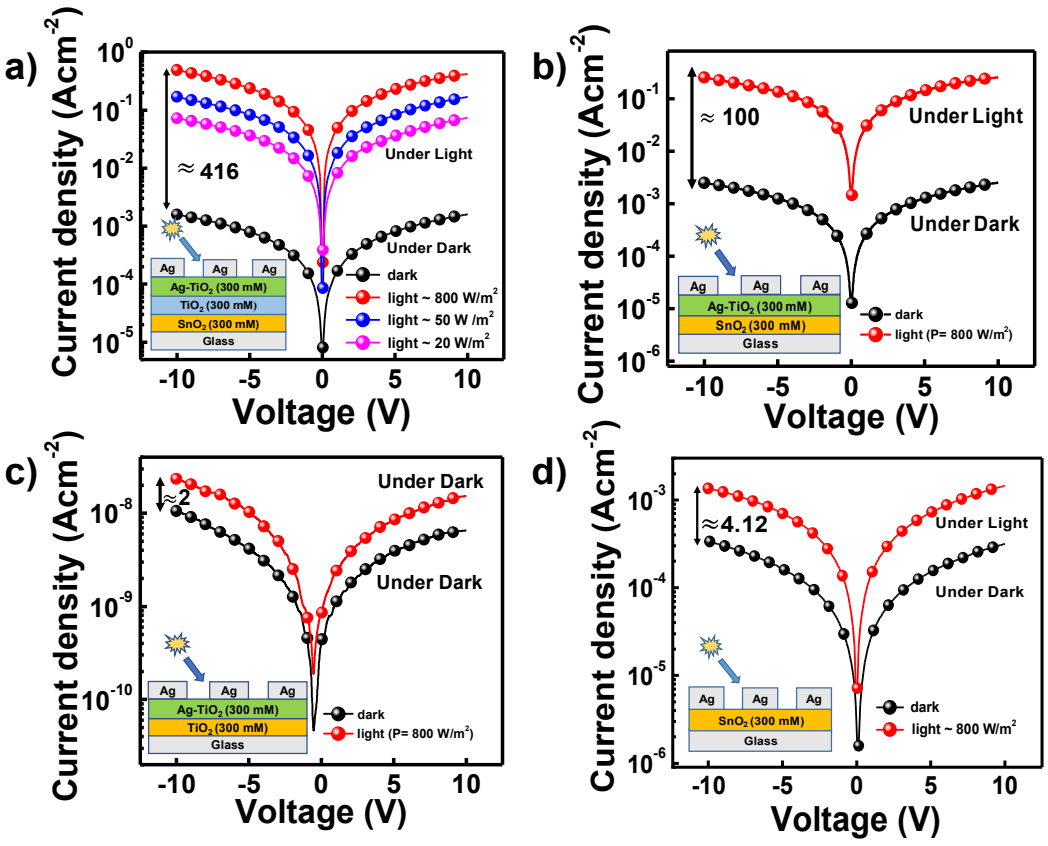

Figure 3.5 Semi-log I-V plot shows the photoconductivity of **a)** Ag-$TiO_2/TiO_2/SnO_2$ **b)** Ag-TiO_2/SnO_2 **c)** Ag-TiO_2/TiO_2 and **d)** SnO_2 based device under dark and light illumination.

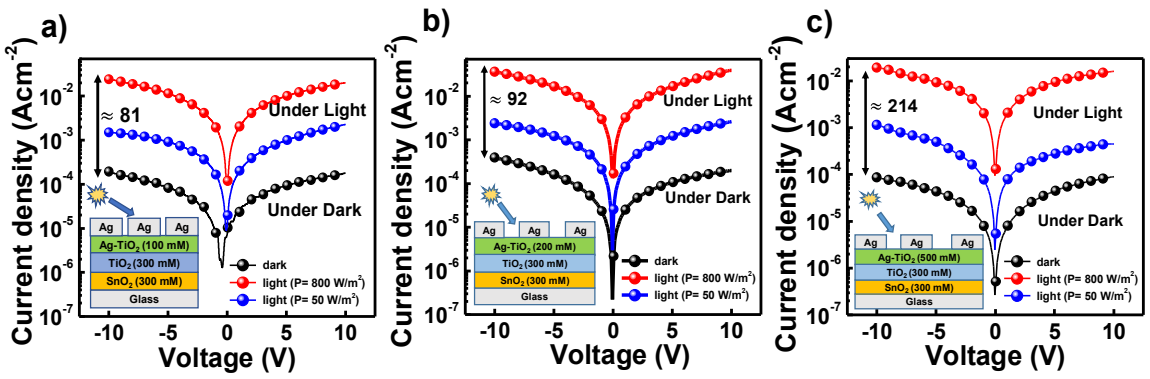

Figure 3.6 I-V plot for different concentration of Ag-TiO_2 layer **a-c)** 100,200 and 500 mM respectively under white light illumination at different intensities.

3.3.4 Experiment Evaluation of EQE & IQE and Role of Plasmon Excitation

Optical excitation must be separated from subsequent electronic transit and collection to experimentally analyze the significance of plasmonic hot electrons in device performance.[171] For this, we experimentally measure EQE within the wavelength range from 300 to 600 nm which describes the incident photon-to-photocurrent generation efficiency which is shown in **Figure 3.7a-d)** for main device (Ag-TiO_2/TiO_2/SnO_2/glass). From this spectrum, it can be noted that, there is a strong photocurrent spectrum in the range 400 to 480 nm with a peak at 420 nm. This spectrum is very much similar to the absorption spectra of Ag-TiO_2 thin film (**Figure 3.2b)**) where we found strong plasmonic absorption in the same region, indicating that the photocurrent of this device is generating mostly due to the hot electron generation from the Ag NPs. With 300 mM concentration of Ag-TiO_2 thin film, we get best photocurrent generation which match with I-V data as well. Here, we also provide different concentration (100,200, and 500 mM) Ag-TiO_2 based EQE data to understand the photocurrent generation more clearly with different thickness of active Ag-TiO_2 layer.

However, during illumination, some part of that incident light is reflected by the Ag-TiO_2/TiO_2/SnO_2 thin film which needs to be excluded to understand the role of the hot-electron generation in this plasmonic photodetector. Therefore, to recognize the contribution

of hot electron on the photocurrent generation of the device, IQE data has been extracted from the experimentally determined EQE data by using **Equation 2.13**.

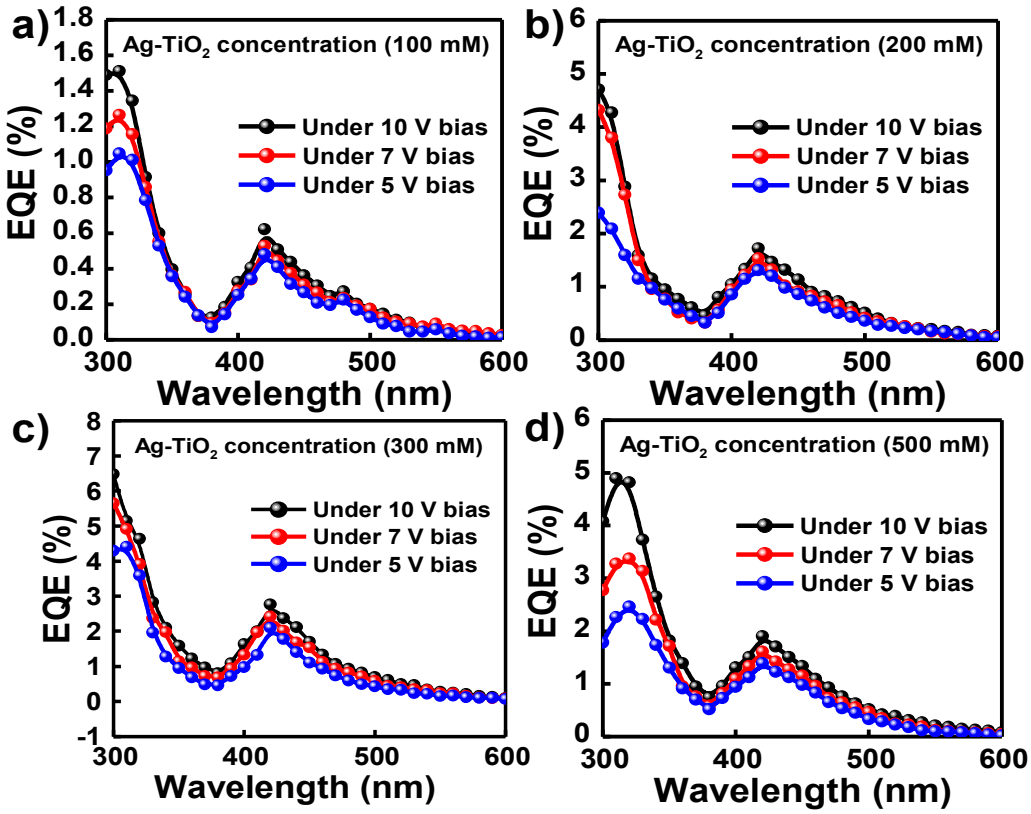

Figure 3.7a-d) EQE data of the plasmonic Ag-TiO_2 thin film based hot electron photodetector for different concentration of Ag-TiO_2 (100,200,300 & 500 mM).

The extracted IQE spectrum has been shown in **Figure 3.8a)**, indicating much stronger photocurrent generation in the plasmonic absorption spectra region. The maximum value of IQE is ~ 4.02% at 420 nm which is ~ 1.5 times of EQE value at the same wavelength.

Moreover, it has been observed the EQE of this device depends on the thickness of Ag electrodes and Ag with 30 nm thickness gives the highest photocurrent. As it is known that the transport of these hot carriers to an interface can occur either ballistically or via electron-electron and electron-phonon scattering, therefore the hot carrier collection by the electrodes also depends on it. It has been reported that when the thickness of such plasmonic strips becomes in the order of average mean path of hot carrier (~20 nm), collection of hot carriers

by the electrodes can be ballistically without much scattering. Therefore, in this photodetector, this optimum 30 nm Ag electrode thickness gives the highest photocurrent (**Figure 3.8b)**).

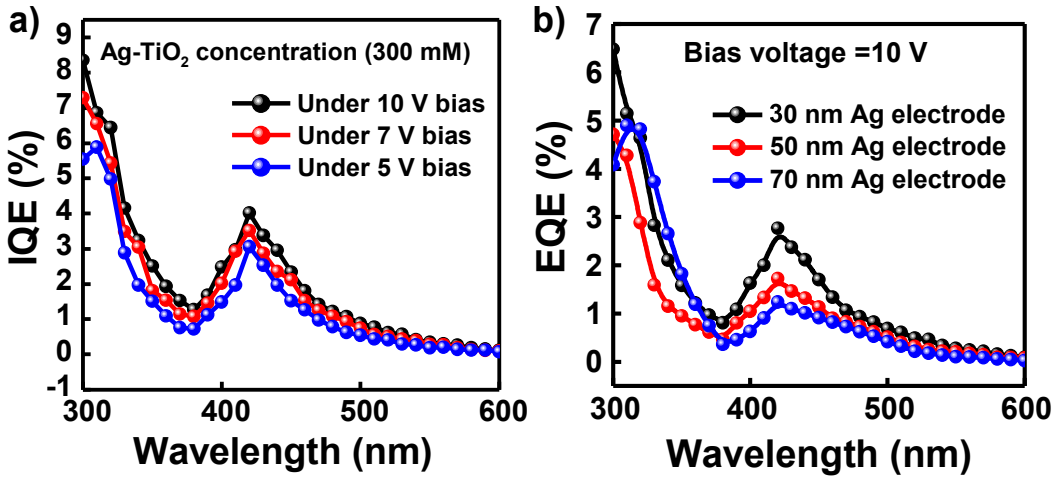

Figure 3.8a) Extracted IQE data of Ag-TiO_2 based hot electron photodetector **b)** EQE data for different thickness of Ag electrode.

In the photocurrent generation process, initially light is absorbed by the material followed by hot electron generation and subsequent transport to the electrodes which is schematically presented in **Figure 3.9a-c)**. Since, the hot electron of Ag NPs is generated from the intraband excitation (s-band) and Ag-TiO_2 Schottky junction has lower barrier height, therefore, hot electrons of Ag NPs can easily transfer to the conduction band of TiO_2. Particularly, this *in-situ* grown Ag-TiO_2 has a highly reduced interface state that enables an efficient charge transfer from Ag NPs to the CB of TiO_2 without much recombination loss. Again, it has been observed that an additional TiO_2 layer of this Ag-TiO_2 thin film generates much higher photocurrent in the device. One possible reason for this is due to the lack of TiO_2 contact in the vertical direction of the Ag-TiO_2 only thin film. Whereas an additional TiO_2 ensures a hot electron to get the Ag-TiO_2 interface during the charge transport to the SnO_2 layer. As soon as a hot electron reaches the SnO_2 layer, it increases the electron density of this semiconducting layer and is collected to the electrode under external bias due to its high electron mobility.

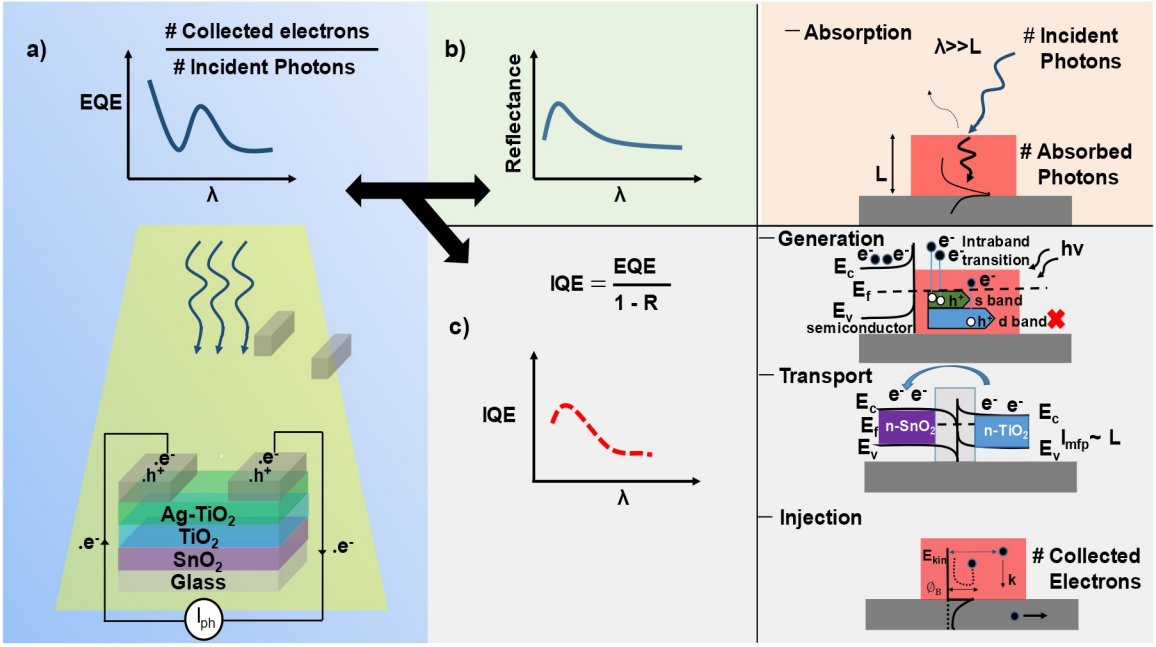

Figure 3.9 Steps of photocurrent generation **a)** EQE spectrum represents the wavelength (λ) - dependent photon-to-electron conversion probability **b)** reflectance data with the variance of different wavelength **c)** schematic representation of IQE which contribute to the carrier generation through intraband transition of Ag NPs. On the other hand, absorption spectrum of a metal nanostructure displaying a resonant plasmonic feature which can be engineered through photonic design. Plasmon excitation indeed yields high absorption in metallic nanostructure switch characteristic dimension L much smaller than the wavelength λ of the incident photon; illustrative IQE spectrum shows the generation of hot charge carriers through intraband transitions, propagation, and scattering of the hot carriers with energy-dependent mean free path (l_{mfp}), and injection of hot carriers with adequate kinetic energy (E_{kin}) and momentum (k) across the Schottky contact ($\emptyset_B$).

3.3.5 Photodetector Device Performance

Responsivity (R_λ) and detectivity (D*) are two key parameters to identify the quality of a photodetector. The EQE, is the photocurrent per photon whereas R_λ is the amount of photocurrent that a unit area photodetector generates when unit power of light is illuminated

on it. Responsivity of the device is calculated from EQE measurement by using **Equation 1.3**.

The change in photo-responsivity of this photodetector under various external biases is depicted in **Figure 3.10a)** for proposed device (Ag-TiO_2/TiO_2/SnO_2/glass) with 300 mM Concentration of Ag-TiO_2 thin film. This data indicates, under an external bias of 10 V, the maximum responsivity of 0.98 (A/W) at 420 nm can be achieved.

The specific detectivity, D*, of a photodetector is a measurement of the signal-to-noise ratio across a 1 Hz bandwidth normalized to the detector's area. It is an essential device parameter that can be used to identify the sensitivity of detectors. By considering the noise that comes mostly from the dark current of the device, detectivity can be measured by using **Equation 1.4.**

The variation of detectivities of proposed heterostructure device are shown in **Figure 3.10b)** under different external bias. The highest detectivity of this heterojunction photodetector is observed with a value of 3.19×10^{11} Jones at 420 nm under 10 V external bias. The peak position of detectivity at 420 nm, indicating the highest sensitivity of device, matches exactly with the plasmonic absorption peak. Therefore, the photocurrent of this device is mostly generated from the hot electron of Ag NPs.

Another important feature of photoconductors is the device's response speed that determines how fast the detector can measure the next signal. The instantaneous response of such devices is further investigated by lighting them with white light pulses of width and separation ~10 s while the device is subjected to a 10 V external bias, as illustrated in **Figure 3.10c)**. The time intervals needed for the photocurrent to increase from 10% to 90% of its peak value (τ_r) and for the response to decrease from 90% to 10% of its peak value (τ_f) are always used to define the device rise time (τ_r) and fall time (τ_f). **Figure 3.10d)** indicates the rise time of the device is ~ 1.2 s and whereas decay time is ~ 0.95 s. This data reveals that the device's rise and decay time responses are reasonably fast. Moreover, the device has been stored in an ambient atmosphere for months, although its photosensitivity and response speed remain almost the same.

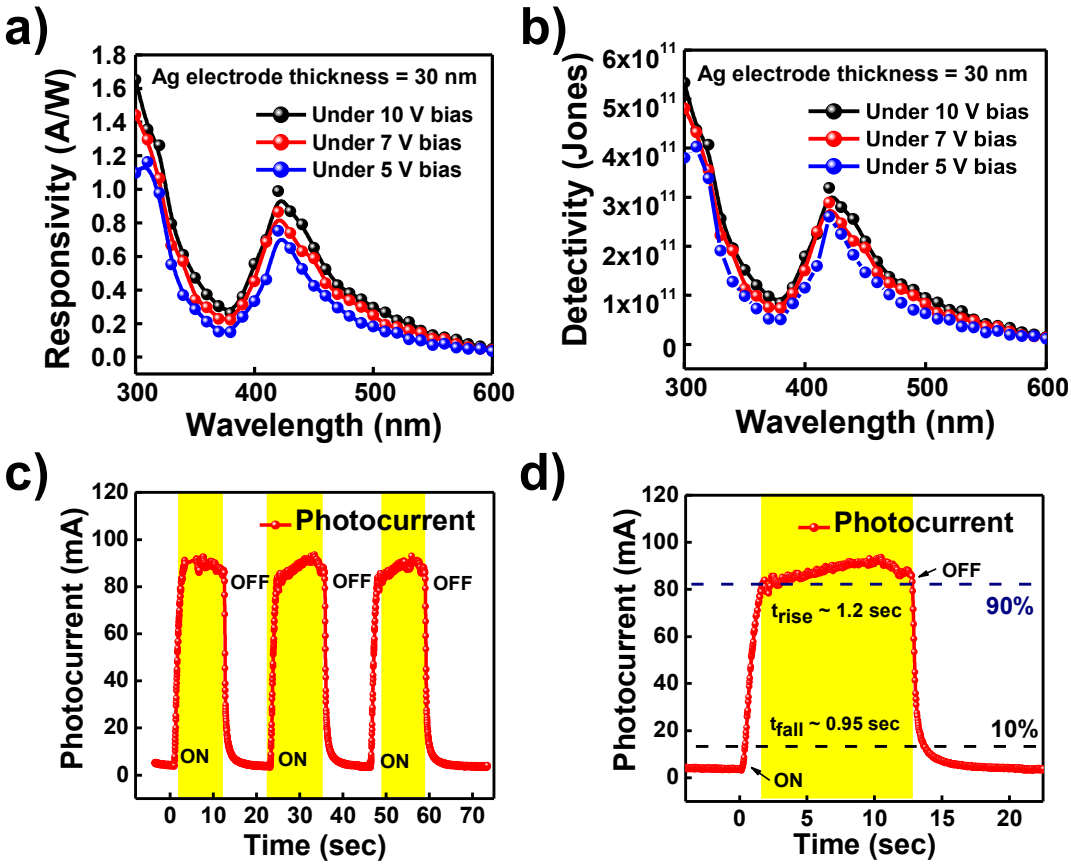

Figure 3.10 illustrates the performance of Ag-TiO_2/TiO_2/SnO_2/glass-based proposed lateral heterostructure photoconductor device **a)** extracted responsivity ($\mathbf{R_\lambda}$) vs wavelength **b)** extracted detectivity (D*) vs wavelength **c)** shows the instantaneous time response of the device **d)** indicates very fast rising and decaying time of ~1.2 s and ~0.95 s, respectively.

To compare the overall performance of our device, a summary of earlier reported works on this plasmonic photodetector is shown in **Table 3.1.** Previous works on hot electron based photodetector have mostly concentrated on responsivity (R_λ) of the photodetectors, while other important parameters of the hot electron photodetectors such as EQE (%), detectivity (D*) and response time (τ_r/τ_f) have not explored much. Out of diferent hot-electronbased photodtector, we found only one work on Ag/TiO_2 based material in photodiode geometry (Nanophotonics. 2019;8(7):1247-1254.) that have faster response time due to its photodiode gemetry. They didn't report the EQE and detectivity spectrum of the device in that paper,

but mention the peak detectivity value which is added in the table. In comparison to those reported hot-electron photodetectors, our Ag-TiO_2 based hot electron photodetector exhibits a higher responsivity whith higher detectivity value. Additionally, our strong narrowband response which can be utilized as colour sensitive photodetector.

Table 3.1 Comparison of the present Ag-TiO_2 based photodetector's device performance with that of other plasmonic hot-electron photodetectors

Device	λ (nm)	EQE (%)	R (A/W)	D^*(Jones)	τ_r/τ_f	Ref.
Ag-TiO_2/TiO_2/SnO_2	420	2.76%	0.98	3.19×10^{11}	1.2/0.95 s	This Work
Porous Ag/TiO_2	450	–	3.3×10^{-3}	9.8×10^{10}	112/24 µs	[165]
Ag/TiO_2 NTs/FTO	370	–	176.30	–	82/14 s	[172]
Porous Au/Si	–	–	3.5×10^{-3}	–	–	[173]
Au nanorods/Si	–	–	1.0×10^{-5}	–	–	[154]
Au/Pyramid-Si	1200	–	8.2×10^{-3}	1.8×10^{10}	–	[159]
Au/ $SrTiO_3$/Si	1350	–	3.7×10^{-4}	–	1 ms	[174]

3.4 Conclusions

In conclusion, in this chapter, we presented a highly efficient Ag-TiO_2 nano-heterostructure based hot electron photodetector, which had a narrowband response in the visible region with a fast response speed. Device has been fabricated in solution-processed techniques in photoconductor geometry. The responsivity, EQE and detectivity of this photodetector at 420 nm are calculated to be 0.98 A/W, 2.76% and 3.19×10^{11} Jones respectively, whereas transient photocurrent study indicates its rise and fall time are 1.2 s and 0.95 s respectively. The detectivity of this plasmonic photodetector has been compared with earlier reported works which reveal superior photosensitivity of this detector, which becomes possible due to the efficient hot electron transfer through the Ag-TiO_2 nano-heterostructure. Besides, using an underlying SnO_2 charge transport layer, photo-generated electrons are collected efficiently to the electrodes. Overall, device performance of this photodetector gives a visible way to fabricate narrowband photodetectors using plasmonic NPs.